ACCEPTED MANUSCRIPT
Final published version of this article: PHYSICAL REVIEW B 82, 195420 (2010)
DOI: https://doi.org/10.1103/PhysRevB.82.195420

Layer-dependent Debye temperature and thermal expansion of Ru(0001) by means of high-energy resolution core-level photoelectron spectroscopy

Eugenio Ferrari,[1] Lorenzo Galli,[1] Elisa Miniussi,[1] Maurizio Morri,[1] Mirko Panighel,[1] Maria Ricci,[1] Paolo Lacovig,[2] Silvano Lizzit,[2] and Alessandro Baraldi[1,3,*]

[1] Physics Department, University of Trieste, Via Valerio 2, I-34127 Trieste, Italy
[2] Sincrotrone Trieste S.C.p.A., Strada Statale 14 Km 163.5, 34149 Trieste, Italy
[3] Laboratorio TASC, IOM-CNR, S.S. 14 Km 163.5, I-34149 Trieste, Italy

The layer-dependent Debye temperature of Ru(0001) is determined by means of high-energy resolution core-level photoelectron spectroscopy measurements. The possibility to disentangle three different components in the Ru $3d_{5/2}$ spectrum of Ru(0001), originating from bulk, first-, and second-layer atoms, allowed us to follow the temperature evolution of their photoemission line shapes and binding energies. Temperature effects were detected, namely, a lattice thermal expansion and a layer-dependent phonon broadening, which was interpreted within the framework of the Hedin-Rosengren formalism based on the Debye theory. The resulting Debye temperature of the top-layer atoms is 295±10 K, lower than that of the bulk (T = 668±5 K) and second-layer (T = 445±10 K) atoms. While these results are in agreement with the expected phonon softening at the surface, we show that a purely harmonic description of the motion of the surface atoms is not valid, since anharmonic effects contribute significantly to the position and line shape of the different core-level components.

I. INTRODUCTION

The determination of the Debye temperature θ_D of solid surfaces, which is related to the dynamic motion of atoms, is extremely important for understanding the new physical properties arising when the translational symmetry of a three-dimensional solid is broken. Surface melting is perhaps one of the most important examples.1,2 The temperature at which the abrupt change from a crystalline to a liquid phase takes place can be simply estimated using the Lindemann criterion: surfaces melt when the square root of the atomic mean-square displacement $<u^2>$ due to thermal vibrations is a sizeable fraction (about 15%) of the lattice parameter.3,4 In the Debye model $<u^2>$ is directly linked to θ_D by the equation $<u^2>=9\hbar^2T/mk_B\theta_D^2$. Therefore its layer-dependent determination permits to understand whether surface atoms melting occurs at significantly lower temperature than in the bulk.

The experimental determination of the Debye temperature is commonly based on scattering (lowand medium-energy ion scattering,5 atomic beam scattering6,7) and diffraction [x-ray diffraction,8,9 low-energy electron diffraction (LEED) (Refs. 10–12)] techniques, where the attenuation of the diffracted beam intensity with increasing temperature is exploited. Moreover, the Debye temperature is a key ingredient in the surface structural determination since it enters the parameter refinement and optimization when comparing experimental and calculated diffracted beam intensities.

In the past, the different surface sensitivity of electrons and x-rays allowed comparing the relative amplitude of thermal vibrations of surface and bulk atoms. When used at different electron beam energies, even LEED is a powerful method to probe the changes in effective Debye temperature, because of the varying electron inelastic mean-free path.13 To date, these methods have allowed to

extend the determination of the Debye temperature, which is usually restricted to surface and bulk atoms, also to subsurface layers only for few systems.11,14

There are several points supporting the idea that the Debye temperature of second-layer atoms should be different than that of bulk and surface layers. In fact, the anisotropic motion of surface atoms and the interlayer relaxation, which is temperature dependent, can appreciably modify the force constants on second-layer atoms. As a consequence, the latter should exhibit a behavior intermediate between that of bulk and first-layer atoms. However, the accurate determination of the layer-dependent Debye temperature is a very demanding task. Diffraction techniques, which have been extensively used in structural investigations of surfaces and interfaces, perform very well on ordered systems, but convey a long-range averaged information and may therefore encounter limitations in probing nonequivalent local atomic arrangements. This is why an unambiguous determination of the parameters describing the thermal motion in different layers is not always straightforward. Therefore an alternative method to estimate the layer-dependent Debye temperature would be important.

In the present study we employ the high-energy resolution core-level x-ray photoelectron spectroscopy (XPS) technique based on synchrotron radiation to determine θ_D for the Ru(0001) surface, second-layer and bulk atoms. This approach exploits the fact that the core levels of a metal can be split into different components which originate from different layers. The binding energy (BE) shift of the surface component relative to the bulk, named surface core-level shift (SCLS),15 is closely related to the local electronic density of states and thus provides valuable information about the electronic structure of clean as well as of adsorbate-covered metal surfaces. Noteworthy, there are several examples where even subsurface core level shifted components have been detected, as in the case of Be,16–21 Ta,22 W,23,24 Rh,25–27 and Ru.28–30

One further reason supporting the core-level photoemission approach is that, according to previous studies, SCLS measurements are a valuable tool to probe bulk and surface Debye temperature.31–34 In fact, by applying the Debye model for the local phonon density of states within the harmonic approximation and the linear electron-phonon coupling, Hedin and Rosengren35 (HR) derived the following expression for the phonon broadening of core-level peaks as a function of the temperature T,

$$G^2(T) = G_{res}^2 + G_{inh}^2 + G_{ph}^2(0)\left[1 + 8\left(\frac{T}{\theta_D}\right)^4 \int_0^{\theta_D/T} \frac{x^3}{e^x - 1} dx\right], \quad (1)$$

where $G(T)$ is the temperature-dependent Gaussian width of the core-level components, G_{res} and G_{inh} are the contributions of the instrumental resolution and inhomogeneous broadening, respectively, $G_{ph}(0)$ is the phonon broadening at $T = 0$ K and θ_D is the Debye temperature.

In this work, we apply the HR theory to the analysis of the Gaussian widths of the bulk, first-, and second-layer components, as determined by fitting the Ru $3d_{5/2}$ core-level spectra of Ru(0001) measured at different temperatures.

II. EXPERIMENTAL

The measurements were performed at the SuperESCA beamline36 of the Elettra synchrotron radiation facility in Trieste, Italy. The photoemission spectra were collected by means of a Phoibos 150 mm mean radius hemispherical electron energy analyzer from SPECS, equipped with in-house developed delay line detector.

The experimental setup combines high-energy resolution with high data acquisition rates, thus allowing to monitor in real time the evolution of the core-level spectral components over a wide temperature range. The overall experimental energy resolution (which accounts for both the electron energy analyzer and the x-ray monochromator) was always kept within 50 meV in all measurements, as determined by probing the width of the Fermi level of a Ag polycrystal.

The Ru(0001) single crystal was mounted on a liquidhelium cryostat manipulator with four degrees of freedom. The sample was cooled by liquid nitrogen and heated by electron bombardment from hot tungsten filaments mounted behind it. The temperature of the sample was monitored by means of two K-type thermocouples directly spotwelded on one side of the specimen.
The sample was cleaned by repeated cycles of Ar^+ sputtering and oxygen treatments, followed by annealing to 1600 K to remove residual oxygen. The ordering and cleanliness of the surface were checked by LEED, which exhibited a sharp (1 x 1) pattern with low background intensity, and by XPS. The procedure was always repeated after annealing to high temperature, which could induce irreversible surface contamination.
When performing high-resolution SCLS measurements, a very good background pressure is required, since even a tiny amount of impurities (mainly hydrogen, water and carbon monoxide, which are typical contaminants in a ultra high vacuum environment) may alter the line shapes and BEs of the core-level components, as well as cause the appearance of new features. This is the reason why the pressure was always maintained below $1.5x10^{-10}$ mbar during measurements.
In the first part of the experiment, high-resolution Ru $3d5_{/2}$ spectra were acquired in sweep mode, i.e., by scanning the energy of the analyzer, at low temperature, in order to minimize thermal broadening effects and make an accurate determination of the line-shape parameters. In the second stage, we investigated the temperature effects on the spectral linewidths and on the core-level BEs by performing a series of fast XPS measurements, in which the evolution of the Ru $3d5_{/2}$ core levels was monitored while the sample was cooling down from high temperature. The spectra were acquired in two modes, namely, in sweep mode and in fixed mode. In the latter case, instead of scanning the analyzer voltages, “snapshot” spectra are obtained by exploiting the energy dispersion of the analyzer at the detector plane. As will be explained in more detail in the next section, this acquisition mode, combined with the large number of virtual channels of the detector (more than 800 points per spectrum) that guarantees accurate measurements of the spectral line shapes even for dwell times of 1 s or shorter, gave the possibility to obtain a more uniform sampling over the whole temperature range considered.
It is important to stress that these experiments are extremely demanding in terms of energy resolution, surface sensitivity, signal-to-noise ratio and data acquisition rates. Care must be taken in order to avoid small perturbations of the experimental conditions, e.g., due to photon beam instabilities or residual magnetic fields, which may affect the spectral line profile.

III. RESULTS

A. High resolution low-temperature measurements

Prior to the temperature-dependent measurements, we collected and analyzed a series of high-resolution Ru $3d5_{/2}$ spectra at low temperature (80 K), where thermal smearing effects are minimized, in order to pinpoint the BEs and lineshape parameters of the core-level components. We spanned different photon energies in the range 350–400 eV, and worked in three angular configurations: at normal emission, at grazing emission (70° from the surface normal) and in the forward scattering geometry37 (about 36° from the surface normal), where an atom of the first-layer lies in line between a second-layer emitter atom and the electron energy analyzer. This strategy, which has already been successfully applied in previous works,26,29,30,34 proved extremely useful to facilitate the spectral deconvolution in the subsequent data analysis.
All the spectra were fitted to Doniach-Šunjič (DS) functions convoluted with a Gaussian distribution. The DS profile combines a Lorentzian width Γ, which is related to the finite core-hole lifetime, with the Anderson singularity index α, which reflects the occurrence of electron-hole pair excitations. The Gaussian width accounts for phonon broadening, instrumental resolution, and any inhomogeneous broadening. The background was assumed to be linear. The reported BE positions of the spectra were calibrated with respect to the Fermi level, which was measured under the same conditions. The data analysis allowed us to unambiguously identify three Ru $3d5_{/2}$ core-level components, consistently with what reported in previous investigations.29,30

Besides the bulk contribution, we identified a surface component, which is shifted to lower BE, as expected for a *d* metal with a more than half-filled *d* band, 38 and a secondlayer component, which appears like a shoulder at higher BE than the bulk. While the identification of the surface component was straightforward, owing to the relatively large SCLS, the deconvolution of the bulk and second-layer components was not trivial, since they lie very close to each other. By properly tuning the photon energy and the photoemission angle, it is possible to induce an intensity modulation of the three core-level components, due to diffraction effects and to the energy-dependent photoelectron mean-free path in the solid.

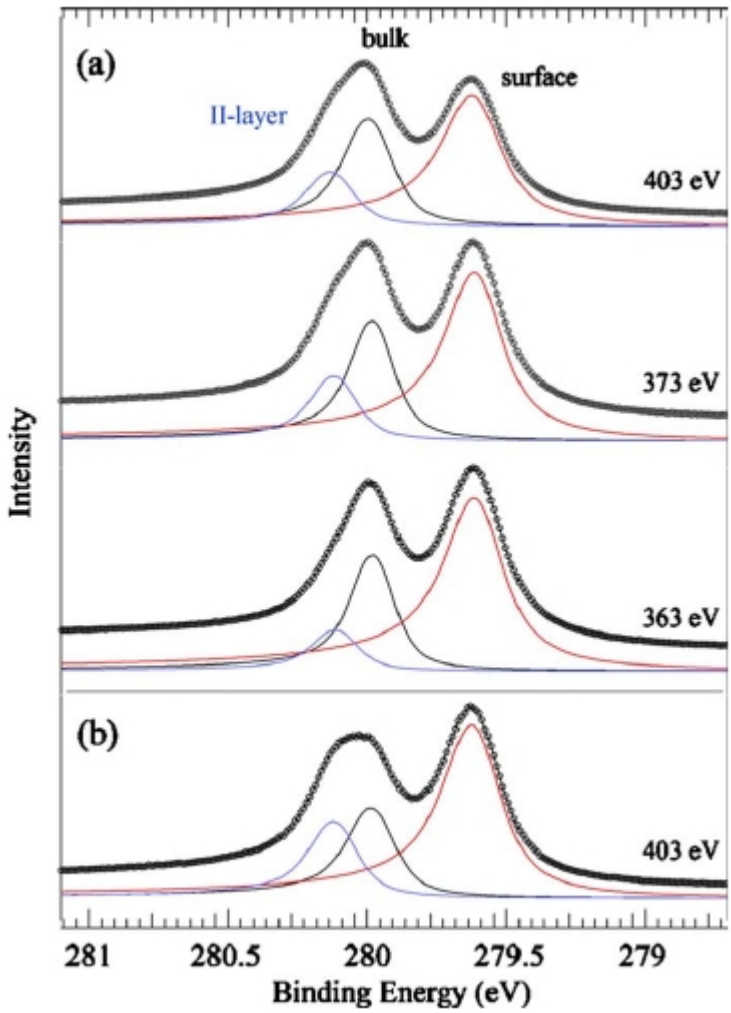

FIG. 1. Selected high-resolution Ru $3d_{5/2}$ spectra measured at different photon energies and photoemission angles (T = 80 K). The spectra are acquired at (a) normal emission and (b) in forward-scattering geometry. The deconvolution into bulk, surface, and second-layer components is shown superimposed.

Figure 1(a) shows a selection of Ru $3d5_{/2}$ spectra collected at normal emission at different photon energies, together with their deconvolution into bulk, surface, and second-layer components. As can be clearly seen, the intensity of the surface feature is enhanced at lower energies while an opposite trend is observed for the bulk component. The second-layer photoemission signal, on the other hand, keeps an almost constant intensity at all photon energies. In Fig. 1(b) is shown a spectrum acquired at 403 eV in the forward-scattering geometry. A comparison with the spectrum measured at normal emission at the same photon energy highlights a different ratio between the intensities of the bulk and second-layer components, which amounts to 1.9 at normal emission, while it drops to 1.2 in the forward-scattering geometry. In the following, we will focus, in particular, on the analysis of

the Ru $3d_{5/2}$ spectra acquired at $h\nu$ = 403 eV, both at normal emission and in the forward-scattering geometry.

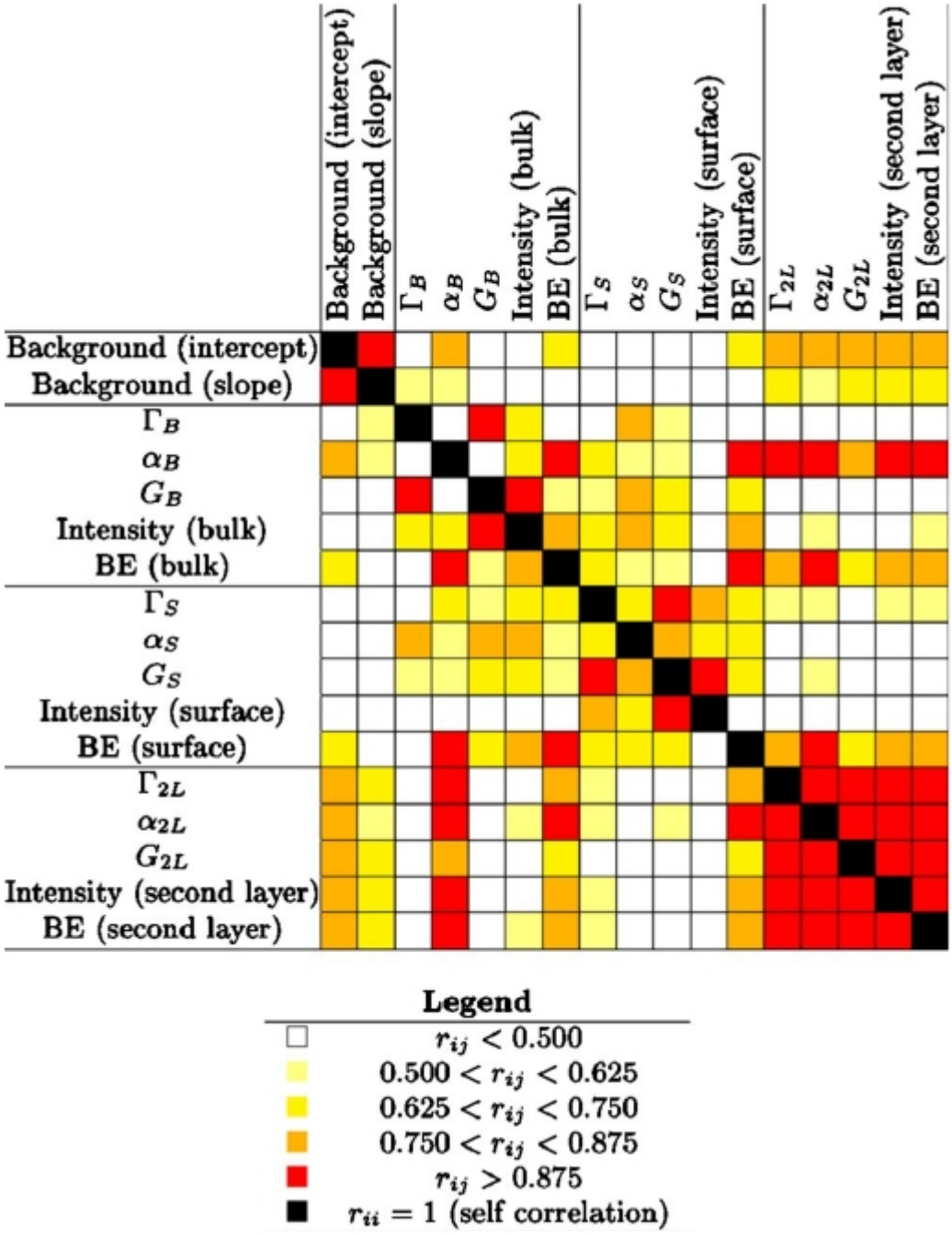

FIG. 2. Correlation matrix for the fitting coefficients of the Ru $3d_{5/2}$ spectrum acquired at normal emission and $h\nu$ = 403 eV. r_{ij} describes the degree of correlation between the parameters i and j.

Collecting a series of spectra at different photon energies and in different angular configurations allows to detect and subsequently remove possible correlation effects between the fitting parameters. A quantitative tool to assess the degree of correlation between two fitting coefficients is provided by the correlation matrix, i.e., the normalized form of the covariance matrix. The correlation matrix for the set of fitting coefficients of the Ru $3d5_{/2}$ spectrum acquired at normal emission for $h\nu$ = 403 eV is reported in Fig. 2; the color scale reflects the degree of correlation between any pair of terms (see legend). A high degree of correlation between two parameters is typically reflected in an unphysical modulation of the latter upon changing the photon energy and

the photoemission angle. This behavior was indeed observed in a preliminary trial fit, in which we left all parameters unconstrained.
An efficient strategy to remove fictitious correlation effects, which has already been successfully tested in previous works,22,26 is given by the analysis of the chi-square (χ^2) contour plots, in which the evolution of the χ^2 is mapped while two fitting coefficients are simultaneously varied.

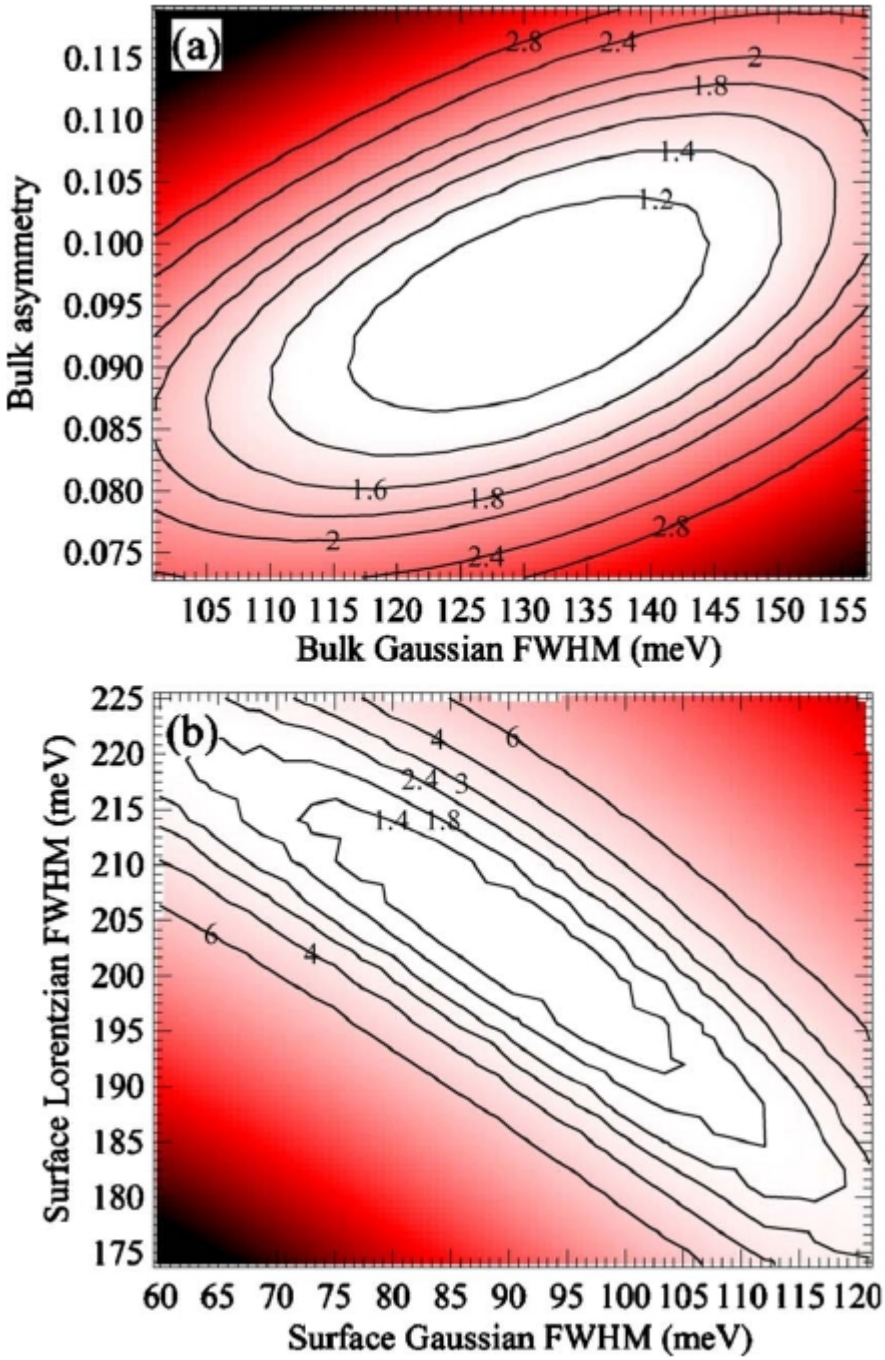

FIG. 3. Two-dimensional contour plots referred to the fit of Ru $3d_{5/2}$ core-level spectrum measured at $h\nu$ = 403 eV at normal emission. The plots show the normalized chi square χ^2/χ_{MIN}^2 as a function of (a) asymmetry and Gaussian width of the bulk component and (b) Lorentzian and Gaussian width of the surface component.

The presence of a deep and localized minimum in the phase space diagram indicates that the optimum value of the parameters lies in the range where the minimum is found. Figure 3 shows two contour plots for the spectrum acquired at $h\nu$ = 403 eV at normal emission, where the quantity

χ^2/χ_{MIN}^2 is plotted in color scale. This method provided us also a tool to estimate the error bar affecting the fitting parameters: for each contour plot, we selected the region were the χ^2 lay within 5% from its minimum value and calculated the corresponding range of variation in the fitting coefficients.

Although, in principle, a different line shape would be expected for bulk and second-layer components, the two peaks lie so close to each other, and their fitting coefficients are therefore so highly correlated, that no reliable estimate could be derived for two distinct sets of line-shape parameters. Hence, in order to reduce the number of degrees of freedom, we constrained the bulk and second-layer components to a common set of line-shape parameters.

The results of the analysis are summarized in Table I. The fitting procedure used proved successful, as reflected in the structureless modulation of the residuals for all spectra (not shown). We found a firstand second-layer CLS of −375±5 meV and +135±5 meV, respectively, which are in good agreement with previously published results.29,30

As to the line-shape parameters, a first interesting result concerns the larger Gaussian width of the bulk and secondlayer components compared to that of the surface. Intuitively, an opposite behavior would be expected, since phonon excitations are enhanced at the surface, owing to the lower coordination of top-layer atoms. In similar cases, it has been surmised that the presence of buried features close to the bulk peak is responsible for the observed Gaussian broadening of the bulk and second-layer components. Only in few cases, where a direct comparison with theoretical calculations was available, it has been possible to disentangle the individual contributions of third and deeper layers from that of the bulk.16,17,19,21 In general, however, the CLSs of the former fall below the attainable experimental resolution, so that these contributions remain hidden, thus leading to a fictitious broadening of the other components. An alternative explanation has been proposed by Riffe et al.,39 who investigated the Ta(100) surface. Following the HR model,35 they pointed out that, in a first-order approximation, the intrinsic Gaussian broadening of a core-level component is related to the temperature by the following expression [compare Eq. (1)]:

$$G_{ph}^2 \simeq \frac{C}{\Theta_D}\left[1+\left(\frac{8}{3}\frac{T}{\Theta_D}\right)\right], \qquad (2)$$

where C is a constant that depends on the details of the valence band structure and on the mass density of the solid; therefore it is not necessarily the same for surface and deeper layer components. This issue, anyhow, is still an open question at present.

TABLE I. Fitting parameters obtained for Ru $3d_{5/2}$ spectra measured at $h\nu$ = 403 eV.

Fitting parameters	Normal emission	Forward scattering
Bulk and second-layer Lorentzian FWHM (meV)	115 ± 15	120 ± 20
Bulk and second-layer asymmetry	0.095 ± 0.005	0.105 ± 0.015
Bulk and second-layer Gaussian FWHM (meV)	130 ± 10	125 ± 15
Surface Lorentzian FWHM (meV)	205 ± 10	185 ± 10
Surface asymmetry	0.115 ± 0.010	0.110 ± 0.015
Surface Gaussian FWHM (meV)	90 ± 10	105 ± 10
Surface core-level shift (meV)	−375 ± 5	−365 ± 10
Second-layer core-level shift (meV)	135 ± 5	135 ± 5

With reference to Table I, another interesting finding is the larger Lorentzian width of the surface compared to that of the bulk and second-layer components. This indicates a shorter core-hole lifetime at the top layer, which can be understood in terms of the lower coordination of surface

atoms. This, in fact, leads to a higher localization of the more atomiclike *d* electrons, which in turn enhances the intra-atomic Auger decay probability. Actually, there are two counteracting effects which should be taken into account. On one hand, an increased delocalization of the *4d* conduction electrons may reduce the overlap between *3d* and *4d* levels and therefore result in a lower Auger decay probability. In addition, the firstto second-layer inward lattice relaxation, which has been reported for this surface,40 and the subsequent bondlength contraction, may mimic the effect of an increased coordination. Nevertheless, according to our results, the latter effects are evidently overridden by the increased localization of *4d* electrons at the top layer. A similar trend [namely, a larger Lorentzian full width at half maximum (FWHM) for the surface than for the bulk component] has been reported in the past also for W(110),41 Ta(100),39 Rh(110), Rh(100),25 and Ir(111).34
Finally, a larger asymmetry index is found for the surface than for the bulk and second-layer peaks: this can be explained by considering the higher surface density of states at the Fermi level, which accounts for an increased electronhole pair excitation probability. A similar behavior was indeed found also for Ta(100),39 Rh(100), Rh(110),25 Rh(111),26 and Ir(111).34

B. Temperature-dependent measurements

Once the analysis of the high-resolution spectra at low temperature was completed, we investigated the thermal evolution of Ru $3d_{5/2}$ core levels. This was accomplished in two steps: (i) by acquiring high-resolution spectra at some selected temperatures in the range 77–973 K, operating the analyzer in scanning mode; (ii) by taking fast XPS spectra, both in sweep mode and in fixed mode (as described in Sec. II), in which the evolution of the Ru $3d_{5/2}$ core level was tracked while the sample was cooling down from 1100 to 80 K.
In the first part of the temperature-dependent measurements, we acquired a set of high-resolution spectra while keeping the sample at some fixed temperatures, with the purpose of studying the thermal broadening of the core-level components. Within the temperature range investigated, phonon excitations yield the main contribution to the spectral linewidth, which is reflected in a Gaussian broadening of the peaks at increasing temperature. Figure 4(a) shows a selection of Ru $3d_{5/2}$ spectra acquired at normal emission at different constant temperatures.
In order to reduce the degrees of freedom, we fitted this data set by fixing the Lorentzian width and asymmetry index of bulk, surface and second-layer components to their lowtemperature value, allowing only their Gaussian width to vary. This choice relies on the basic assumption that, in a first-order approximation, the core-hole lifetime and the electron-hole pair excitation probability do not depend on temperature.
A problem concerning the spectra acquired at fixed temperature arises from the small BE separation of the bulk and second-layer components, which become almost indistinguishable at high temperature under the effect of thermal broadening [see Fig. 4(a)]. If their intensities were left unconstrained, the fitting procedure returned an unphysical estimate of their line-shape parameters and BEs. Hence, in order to remove possible artifacts and to rationalize the analysis, we forced the ratio between the integrated intensities of the bulk and second-layer components to a fixed value over the whole temperature range. We repeated the fitting procedure for five different values of the ratio (ranging between 1.7 and 2.1), to check how this choice affected the quality of the fit. Since no appreciable effect was detected, we took the value of 1.9, which is the ratio found for the low temperature spectra, acquired at normal emission and at the same photon energy.
The results of our analysis are reported in Fig. 4(b), where the squared Gaussian widths of bulk, surface and secondlayer components are plotted against the temperature. A linear fit to the data is shown superimposed, to highlight the different slopes of the curves.
The large thermal relaxation experienced by the surface is reflected in an enhanced Gaussian broadening of the corresponding core-level component with respect to the other peaks. The bulk and second-layer Gaussian widths, which are almost the same at low temperature, progressively diverge at increasing temperature, with the subsurface component experiencing a larger broadening.
A major drawback of the kind of measurements just described, where the sample is constantly warmed by filament heating, is the presence of current-induced magnetic fields, which may affect

the spectral profiles as well as the measured BEs. Another problem may be carbon surface segregation from the bulk induced by prolonged heating to high temperature which may affect the spectral line shape and BE. This phenomenon, which occurs significantly between 1000 and 1400 K, has been exploited in recent experimental works to grow an epitaxial layer of graphene on Ru(0001).42 In addition, the limited number of experimental points available over a relatively wide temperature range (~900 K) did not allow a reliable comparison between the experimental results and the predictions of the HR model.

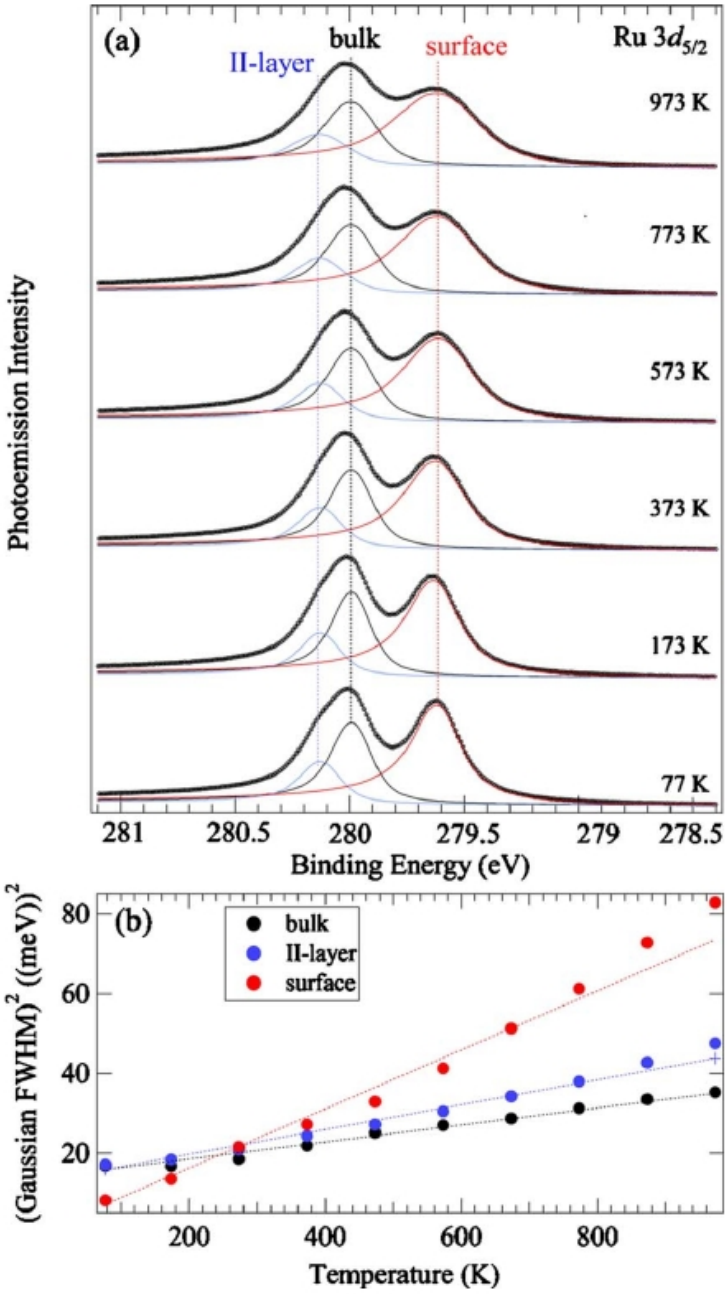

FIG. 4. (a) Selected high-resolution Ru $3d_{5/2}$ core-level spectra acquired at normal emission at different constant temperatures ($h\nu$ = 403 eV). (b) Total squared Gaussian width versus temperature for Ru $3d_{5/2}$ bulk, surface, and second-layer components, as obtained from a least-squares fit to the spectral sequence reported in (a). A linear fit to the data is shown superimposed, as a guide to the eyes.

In order to overcome these problems, we performed fast XPS measurements, in which the thermal evolution of the Ru $3d5_{/2}$ core level was monitored in real time. We first collected a sequence of

spectra in sweep mode while the sample was cooling down from 1100 to 80 K. The result of the data analysis basically confirm the trends we have already observed for the spectra acquired at constant temperature. Also in this case, the surface peak shows an enhanced Gaussian broadening at increasing temperature with respect to the other components. The curves associated to photoemission from the bulk and the second layer, which almost overlap at low temperature, exhibit two distinct trends in the temperature range above 600 K.
However, the scattering of the experimental points in the high-temperature range makes it very hard to correctly resolve the bulk and second-layer contributions at high temperature. Another drawback is that the time required to take each spectrum was about 7 s, which, at the beginning of the cooling run (approximately above 800 K), corresponds to a sizeable temperature drop (approximately 80 K) during each scan: this means that the different BE intervals of the hightemperature spectra are affected by thermal broadening in a nonuniform way.

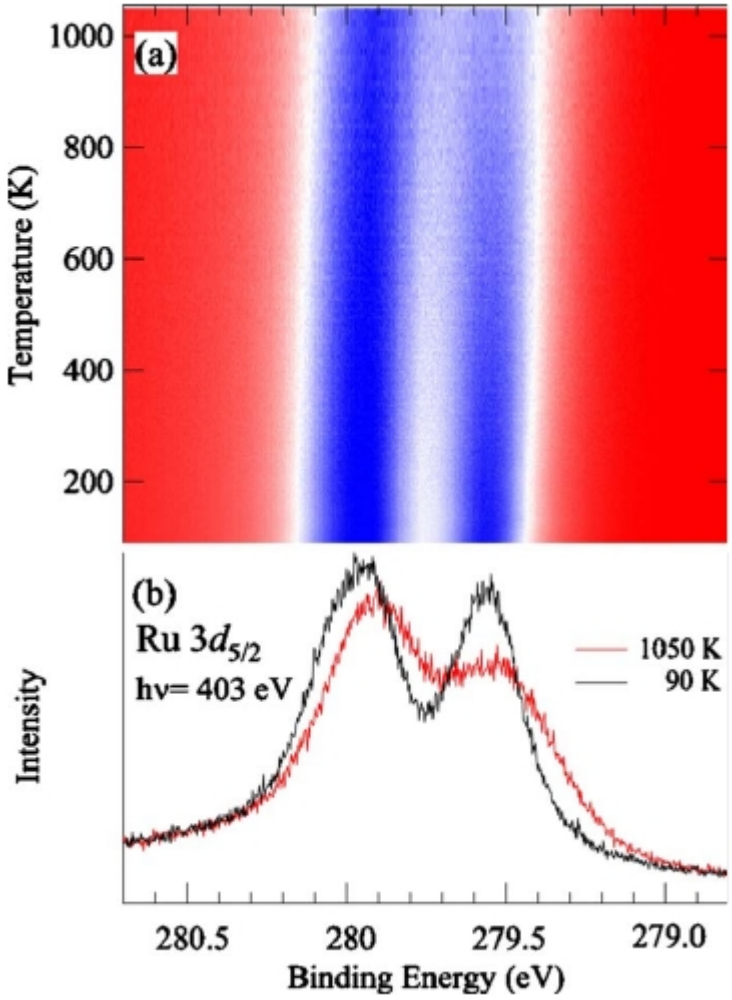

FIG. 5. (a) Thermal evolution of the Ru $3d_{5/2}$ core levels during cooling of the sample (series acquired in fixed mode, at normal emission, and $h\nu$ = 403 eV). The acquisition time is 1 s per spectrum. (b) Ru $3d_{5/2}$ spectra corresponding to T = 1050 K and T = 90 K.

In order to achieve an accurate assessment of the temperature-dependent parameters, we exploited the snapshot operation mode (described in Sec. II) to collect spectra at normal emission and at $h\nu$ = 403 eV, with acquisition time of 1 s per spectrum. This unique operation mode allows a considerably faster acquisition rate compared to sweep mode, which is particularly suitable to tackle the short timescale evolution of core levels. It should be stressed how the faster data acquisition rate not only increased the number of experimental points available over the whole temperature range, but allowed, in particular, a more efficient sampling of the high temperature interval. In addition,

the spectra acquired in fixed mode are much less affected by the temperature drop during each scan than the corresponding sweep mode spectra.
Figure 5(a) shows an intensity plot of the raw data while in Fig. 5(b) two Ru $3d5_{/2}$ spectra acquired at the beginning (T = 1050 K) and at the end (T = 90 K) of the cooling run are reported. Following the same fitting strategy described above, we extrapolated the temperature-dependent Gaussian widths of bulk, surface, and second-layer components (reported in Fig. 6), as well as the thermally induced CLSs of the surface and subsurface components, shown in Figs. 7(a) and 7(b), respectively. The Lorentzian widths and asymmetry parameters were constrained to the values found for the low temperature spectra.
The resulting Gaussian width of the surface component is seen to grow at an appreciably faster rate than the others. Another remarkable observation concerns the Gaussian width of bulk and second-layer components, whose curves are already distinguishable above 400 K.

IV. DISCUSSION

We applied a refined fitting procedure to the data shown in Fig. 6 based on the HR model for the thermal broadening of core-level spectra, as expressed in Eq. (1). In this way, a quantitative estimate of the Debye temperature of bulk, surface, and second-layer Ru could be derived, despite some intrinsic limitations of the model, which will be considered below. The resulting Debye temperature is 295±10 K for the surface, 445±10 K for the second-layer, and 668±5 K for the bulk.
A comparison of these results with those reported in previous works shows an overall good agreement. In particular, Madey et al.43 estimated a surface Debye temperature of 321 K for Ru(0001). These results were obtained by analyzing the intensity attenuation of the LEED spots at increasing temperature for electron-beam energies between 100 and 400 eV. While our estimate of the surface Debye temperature is in agreement with this work,43 a larger discrepancy is found for the bulk Debye temperature (668 K versus 370 K).
This disagreement could be understood by considering that LEED is intrinsically a surface-sensitive technique, so that, even at high kinetic energies, a substantial contribution of the top layer to the overall diffracted intensity cannot be suppressed. Indeed the calculated electron inelastic meanfree path on Ru is found to be only 7.8 Å at 400 eV kinetic energy.44 As a consequence, the value reported by Madey et al. should be considered as an average over the contributions of different layers, including the top layer, which tends to underestimate the actual bulk Debye temperature.
A survey of the experimental data reported in literature shows different values for the Debye temperature of Ru. Calorimetric experiments carried out by Reese et al.45 yielded a Debye temperature of 555±5 K, in good agreement with previous works (Refs. 46 and 47). In a more recent experimental work by Narayana48 the Debye temperature of five different hcp elements was derived from x-ray diffraction data: the estimated Debye temperature of Ru was 495±24 K.
An important remark concerns the range of applicability of the HR model for the different layers. While the model fits the data for the bulk component almost over the whole temperature range, it performs less satisfactorily in the case of the second-layer, for which it provides a suitable description only in the temperature interval below 700 K, and even worse in the case of the top layer for temperatures above 450 K. The failure of the HR model clearly indicates that the simple theory underlying it provides an inadequate description of the thermally induced phonon excitations involving surface atoms. An argument that has often been invoked to explain the anomalous thermal behavior displayed by toplayer atoms is the enhanced anharmonicity of surface vibrations compared to bulk phonon excitations. In general, a purely harmonic description of the motion of the atoms in a solid is not valid, since, as the temperature rises, the amplitude of lattice vibrations increases and the anharmonicity of the interatomic potential is reflected in a thermal expansion of the lattice. Lattice vibrations at the surface are considerably larger than in the bulk, due to the reduced coordination of the atoms, as well as to the boundary condition of vanishing forces at the cleavage plane. The perpendicular motion is expected to be very anisotropic, i.e., with very different potential shape for inward and outward motion, and to become sufficiently excited to reach the anharmonic range even at relatively low temperature. Noteworthy, anharmonicity is responsible for the

anomalous thermal interlayer expansion of solid surfaces and it leads to surface-specific phonondispersion relations.

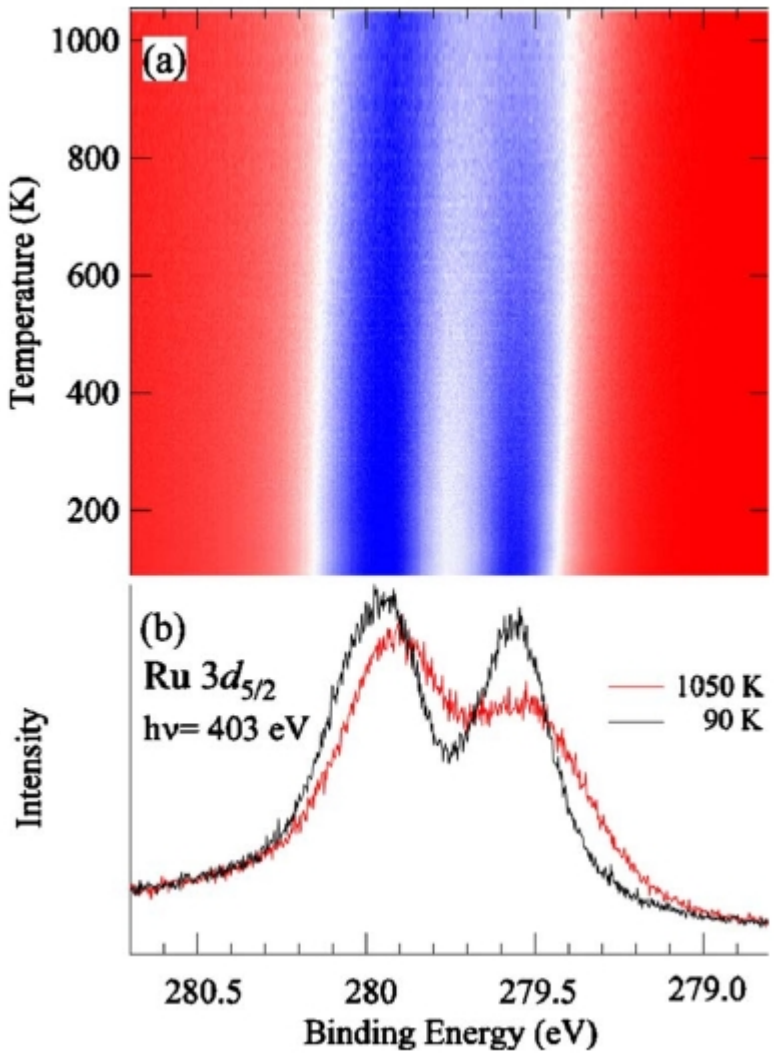

FIG. 6. Squared Gaussian FWHM vs temperature for bulk, surface, and second-layer components, as obtained from a least-squares fit to the time-resolved Ru $3d_{5/2}$ spectral sequence acquired in snapshot mode, at normal emission and $h\nu$ = 403 eV. The fits to the experimental data using the HR model are shown superimposed.

In this framework, extensive investigations have been carried out in the past on the Cu(110) surface.49,50 In this case, an appreciable anisotropy of the vibration amplitudes can be expected due to the twofold symmetry of the structure; for this reason, Cu(110) has been taken as a model system to study surface phenomena such as anharmonicity, roughening transitions, and surface melting.51

In light of these considerations, the apparently odd behavior of the Gaussian FWMH of the surface component (Fig. 6) can be ascribed to increased anharmonic vibrations of toplayer atoms at increasing temperature, which restricts the possibility to apply the HR model to a limited subset of data at low temperature. Moreover, the simple “rule of thumb” stating that the surface Debye temperature should be 1/√2 that of the bulk,52 cannot be applied to our data because it relies on the basic assumption that the atoms in a crystal can be described as harmonic oscillators, which is actually not applicable to our case.

The behavior of the CLSs outlined in Fig. 7 can be interpreted as due to temperature-dependent relaxation of the top layer. While at low temperature the firstto second-layer distance at low temperature is slightly contracted with respect to the bulk interlayer spacing,40 at increasing

temperatures the top-layer undergoes a thermal expansion. It has been indeed observed that most metallic surfaces tend to relax inwards at low temperature while at higher temperatures the contraction turns into an expansion.53 Moreover, the thermal expansion of the first interlayer spacing is considerably larger than in the bulk. This behavior, which has been experimentally observed, e.g., for Pb(110),54 is not surprising if one considers the anharmonic potential felt by a first (or, to a lesser extent, second) layer atom when it is moved along the direction normal to the surface. Again, the large anharmonicity stems from the reduced number of nearest neighbors of first-layer atoms. In this way, the top-layer expansion at higher temperature is responsible for the corresponding SCLS increase, while the second-layer atoms which are “overcoordinated” at low temperature, display a shift to lower BE, thus approaching a more bulk like coordination as the temperature is increased.

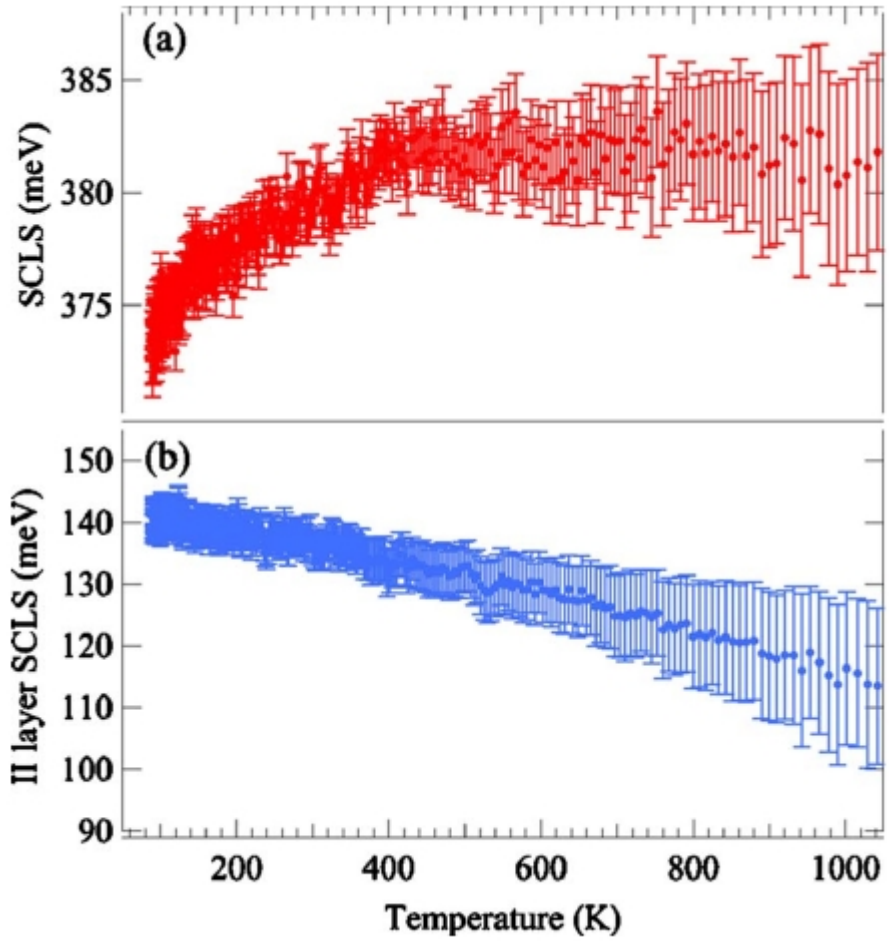

FIG. 7. Thermally induced CLS of (a) surface and (b) second-layer components in the range 80–1050 K, as obtain from a least-square fit to the time-resolved data acquired in snapshot mode, reported in Fig. 5.

The fact that the temperature-dependent SCLS reaches a saturation value approximately above 400 K (see Fig. 7) can be likely related to the onset of anharmonic effects, which are also responsible for the observed breakdown of the Debye model for the surface data above 450 K (see Fig. 6).
The measured BE shifts of the bulk and surface core-level components were used to extrapolate the linear thermalexpansion coefficient (λ) of Ru, by applying the Friedel model which has already been successfully tested on other transition-metal surfaces.39 This model, combined with the linear combination of atomic orbitals (LCAO) calculation of the bandwidth W_d (see Ref. 38), provides an expression for the thermally induced change in the *d*-band center E_d (with respect to the Fermi level) as a function of the normalized linear lattice expansion, $\Delta a/a$ (where Δa is proportional to the temperature variation over the range considered: $\Delta a = \lambda a \Delta T$). The total thermally induced BE shift

(in electron volt) of a core-level component is expressed as the sum of two terms, which account for the contribution of initialand final-state effects, respectively,39

$$\Delta E_{core} = \left\{ 1.1 \frac{W_d(5 - Z_d)}{2} + \frac{10.61}{(r_s/a_0)^{1/2}} \frac{[1 + 1.222(r_s/a_0)^{1/2}]}{[1 + 0.815(r_s/a_0)^{1/2}]^{3/2}} \right\} \frac{\Delta a}{a}, \quad (3)$$

where a_0 is the Bohr radius and rs is given by $V = 4/3\ \pi r_s^3$, V being the volume per conduction electron. We therefore started from the LCAO results of W_d = 8.44 eV and Z_d = 7.27 (Ref. 38) (which implies that Z_s = 0.73 and r_s/a_0 = 3.105) to calculate the expression in braces in Eq. (3). We then used the experimental BE curves of the bulk and surface components to calculate $\Delta a/a$ and plotted the values so obtained against the temperature. A linear fit of the data allowed us to derive the layer-dependent thermal expansion coefficient: in particular, we find a coefficient of $6.26\pm0.07\text{x}10^{-6}$ K^{-1} for the bulk and $9.22\pm0.09\text{x}10^{-6}$ K^{-1} for the top layer. Our results are in good agreement with previous findings. A value ranging between $5.1\text{x}10^{-6}$ and $9.6\text{x}10^{-6}$ K^{-1} is generally found in literature for the linear thermal expansion coefficient of Ru (see Ref. 55). Two distinct values for the thermal expansion coefficient of Ru along the a axis (in-plane lattice expansion, $7.1\text{x}10^{-6}$ K^{-1}) and along the c axis (out-of-plane expansion, $11.1\text{x}10^{-6}$ K^{-1}) are reported in Ref. 56. These data fit our experimental results particularly well. The surface thermalexpansion coefficient evidently receives a larger contribution from lattice relaxation in the direction normal to the plane, due to the lower coordination of top-layer atoms and hence to the larger amplitudes of phonon vibrations at the surface. The smaller thermal expansion coefficient found for the bulk, on the other hand, is consistent with the greater stiffness of deeper layers.

In conclusion we have shown that by using high-energy resolution core-level photoelectron spectroscopy it is possible to obtain an accurate value of the layer-dependent Debye temperature of Ru(0001). Our results show that a harmonic description of the motion of the surface atoms is valid only below 450 K. Above this temperature anharmonic effects contribute significantly to the position and line shape of the different core-level components and result in a different surface and bulk thermal expansion.

ACKNOWLEDGMENTS

A.B. would like to thank the Sincrotrone Trieste S.C.p.A. for providing the access to the Elettra Laboratory and for the support received during the beamtime allocated at SuperESCA beamline, and the Physics Department, University of Trieste for financial support for the course “Laboratorio di Fisica della Materia.” We acknowledge D. Menzel for fruitful discussions and critical reading of the manuscript. A.B. acknowledges precious technical support from Angst-Pfister.

1 U. Tartaglino, T. Zykova-Timan, F. Ercolessi, and E. Tosatti,Phys. Rep. 411, 291 (2005).
2 H. Brune, Ann. Phys. 18, 675 (2009).
3 F. A. Lindemann, Phys. Z. 11, 609 (1910).
4 J. J. Gilvarry, Phys. Rev. 102, 308 (1956).
5 E. van de Riet, J. Fluit, and A. Niehaus, Vacuum 41, 372 (1990).
6 W. H. Weinberg, J. Chem. Phys. 57, 5463 (1972).
7 N. Garcia, A. Maradudin, and V. Celli, Philos. Mag. A 45, 287(1982).
8 C. S. Fadley, Prog. Surf. Sci. 16, 275 (1984).
9 R. Trehan and C. S. Fadley, Phys. Rev. B 34, 6784 (1986).
10 F. C. M. J. M. van Delft, M. J. Koster van Groos, R. A. G. DeGraaff, A. D. Van Langeveld, and B. E. Nieuwenhuys, Surf. Sci.189-190, 695 (1987).

11 U. Löffler, R. Döll, K. Heinz, and J. Pendry, Surf. Sci. 301, 346(1994).
12 D. W. Jepsen, P. M. Marcus, and F. Jona, Surf. Sci. 41, 223(1974).
13 W. W. M. A. Van Hove and C. M. Chan, Low-Energy ElectronDiffraction (Springer-Verlag, Berlin, 1986).
14 E. A. Soares, G. S. Leatherman, R. D. Diehl, and M. A. V. Hove,Surf. Sci. 468, 129 (2000).
15 D. Spanjaard, C. Guillot, M.-C. Desjonqures, G. Treglia, and J.Lecante, Surf. Sci. Rep. 5, 1 (1985).
16 H. I. P. Johansson, L. I. Johansson, E. Lundgren, J. N. Andersen,and R. Nyholm, Phys. Rev. B 49, 17460 (1994).
17 L. Johansson, H. Johansson, E. Lundgren, J. Andersen, and R.Nyholm, Surf. Sci. 321, L219 (1994).
18 L. I. Johansson, P.-A. Glans, and T. Balasubramanian, Phys. Rev.B 58, 3621 (1998).
19 S. Lizzit, K. Pohl, A. Baraldi, G. Comelli, V. Fritzsche, E. W.Plummer, R. Stumpf, and P. Hofmann, Phys. Rev. Lett. 81, 3271(1998).
20J. N. Andersen, T. Balasubramanian, C. O. Almbladh, L. I. Johansson, and R. Nyholm, Phys. Rev. Lett. 86, 4398 (2001).
21 A. Baraldi, S. Lizzit, K. Pohl, P. Hofmann, and S. de Gironcoli,Europhys. Lett. 64, 364 (2003).
22 D. M. Riffe and G. K. Wertheim, Phys. Rev. B 47, 6672 (1993).
23 D. Riffe, G. Wertheim, P. Citrin, and D. Buchanan, Phys. Scr.41, 1009 (1990).
24 G. K. Wertheim and P. H. Citrin, Phys. Rev. B 38, 7820 (1988).
25 M. Zacchigna, C. Astaldi, K. C. Prince, M. Sastry, C. Comicioli,M. Evans, R. Rosei, C. Quaresima, C. Ottaviani, C. Crotti, M.Matteucci, and P. Perfetti, Phys. Rev. B 54, 7713 (1996).
26 A. Baraldi, S. Lizzit, A. Novello, G. Comelli, and R. Rosei,Phys. Rev. B 67, 205404 (2003).
27 A. Baraldi, L. Bianchettin, E. Vesselli, S. de Gironcoli, S. Lizzit,L. Petaccia, G. Zampieri, G. Comelli, and R. Rosei, New J.Phys. 9, 143 (2007).
28 A. Baraldi, S. Lizzit, and G. Paolucci, Surf. Sci. 457, L354(2000).
29 S. Lizzit, A. Baraldi, A. Groso, K. Reuter, M. V. Ganduglia-Pirovano, C. Stampfl, M. Scheffler, M. Stichler, C. Keller, W.Wurth, and D. Menzel, Phys. Rev. B 63, 205419 (2001).
30 S. Lizzit, Y. Zhang, K. Kostov, L. Petaccia, A. Baraldi, D. Menzel, and K. Reuter, J. Phys.: Condens. Matter 21, 134009(2009).
31 D. M. Riffe, G. K. Wertheim, and P. H. Citrin, Phys. Rev. Lett.67, 116 (1991).
32 G. K. Wertheim, D. M. Riffe, and P. H. Citrin, Phys. Rev. B 49,2277 (1994).
33 S. C. Santucci, A. Goldoni, R. Larciprete, S. Lizzit, M. Bertolo, A. Baraldi, and C. Masciovecchio, Phys. Rev. Lett. 93, 106105(2004).
34 M. Bianchi, D. Cassese, A. Cavallin, R. Comin, F. Orlando, L.Postregna, E. Golfetto, S. Lizzit, and A. Baraldi, New J. Phys.11, 063002 (2009).
35 L. Hedin and A. Rosengren, J. Phys. F: Met. Phys. 7, 1339(1977).
36 A. Baraldi, G. Comelli, S. Lizzit, M. Kiskinova, and G. Paolucci,Surf. Sci. Rep. 49, 169 (2003).
37 Here and in the proceeding, we will use the term “forward scattering” only with reference to the geometrical setup of the experiment while the typical energy conditions of an actual forward-scattering experiment were never met in our measurements.
38 W. Harrison, Electronic Structure and the Properties of Solids:The Physics of the Chemical Bond (Freeman, New York, 1980).
39 D. M. Riffe, W. Hale, B. Kim, and J. L. Erskine, Phys. Rev. B51, 11012 (1995).
40 G. Michalk, W. Moritz, H. Pfnür, and D. Menzel, Surf. Sci. 129,92 (1983).
41 D. M. Riffe, G. K. Wertheim, and P. H. Citrin, Phys. Rev. Lett.63, 1976 (1989).
42 S. Marchini, S. Günther, and J. Wintterlin, Phys. Rev. B 76,075429 (2007).
43 T. Madey, H. Engelhardt, and D. Menzel, Surf. Sci. 48, 304(1975).
44 S. Tanuma, C. Powell, and D. Penn, Surf. Interface Anal. 17,911 (1991).
45 W. Reese and W. Johnson, Phys. Rev. B 2, 2972 (1970).
46 K. Clusius and U. Piesbergen, Z. Naturforsch. 14A, 23 (1959).
47 E. S. Fisher and D. Dever, Trans. Metall. Soc. AIME 239, 48(1967).

48 M. Shankar Narayana, N. Gopi Krishna, and D. B. Sirdeshmukh,Acta Cryst. A57, 217 (2001).
49 P. D. Ditlevsen, P. Stoltze, and J. K. Nørskov, Phys. Rev. B 44,13002 (1991).
50 L. Yang and T. S. Rahman, Phys. Rev. Lett. 67, 2327 (1991).
51 W. Moritz, J. Landskron, and M. Deschauer, Surf. Sci. 603,1306 (2009).
52 L. Clarke, Surface Crystallography: An Introduction to Low Energy Electron Diffraction (Wiley, New York, 1985).
53 B. W. Busch and T. Gustafsson, Surf. Sci. 407, 7 (1998).
54 J. W. M. Frenken, F. Huussen, and J. F. van der Veen, Phys. Rev.Lett. 58, 401 (1987).
55 D. R. Lide, Handbook of Chemistry and Physics, 89th ed. (CRCPress/Taylor & Francis, Boca Raton, FL, 2009).
56 G. Beck, Edelmetall-Taschenbuch, edited by A. G. Degussa(Huthig-Verlag, Heidelberg, 1995)